

Impact of wheel ageing on rail corrugation in curve: A parametric study

C. Collette¹, R. Bastais²

Abstract – This paper investigates the impact of the wheel profile aging on the development of rail corrugation. The test case considered for the study is a curved track section from the Brussels metro network (STIB). Rail corrugation is evaluated using a multi-body model of the vehicle and the track. The effect of wheel diameter and shape of the profile are evaluated for the test case considered using the multi-body model.

Keywords: Railway wheel profile, Multi-body model, Stability, Rail corrugation.

I. Introduction

Wheel and rail profiles result from a very long iterative process, started with rectangular profiles and converging to the present day ones. Early evolutions resulted from trial and error processes. Nowadays, algorithms enable to calculate optimal wheel profiles for railway vehicles and test their numerical properties before manufacturing [1][2].

The maximum wear of bogie wheels is defined by geometrical tolerances given by the maintenance department of metro networks. However, these tolerances don't give any information on how old the evolution of the profile shape affects the development of rail corrugation, i.e. if a worn wheel profile gives birth to rail corrugation more rapidly than a new one or not. To this purpose, a test case from the Brussels metro network (STIB) is considered in this paper and described in appendix. The effect of wheel parameters on rail wear is evaluated using a multi-body model of the whole vehicle track system. As a consequence of these better predictions, mainly two recommendations are given to decrease the contribution of the railway wheel profile in the development of rail corrugation.

The paper is organized as follows. Section two presents measurements of STIB wheel profiles. Section three contains general considerations on the effect of profile wear on the vehicle-track dynamics. In section four, the effect of wheel parameters on rail corrugation is evaluated through simulations of the vehicle rolling on the track.

II. Evolution of STIB Wheels

Wheel profiles are characterized by a few parameters (QR, Sh, Sd, SR) defining its main shape (Fig. 1).

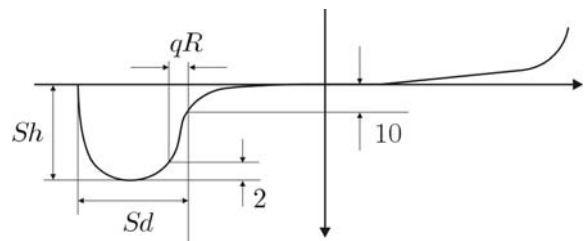


Fig. 1. Wheel profile characteristics.

At STIB, the maintenance department has defined a *warning* value, and a *change* for each of these parameters. The warning value means that the wheel must be grinded; the change value means that the old wheel must be replaced. These values are given in Table I.

TABLE I
TOLERANCES FOR STIB WHEEL PROFILE.

Parameter	Range	Action
QR	[6,5,8] mm	Grinding
QR	< 6.5 mm	Change
Sd	< 22 mm	Grinding
Sh	[36,37] mm	Grinding
Sh	>37 mm	Change

Starting from these tolerances, next section outlines the first approach chosen for the study.

The test case considered is a track section from the STIB metro network, from station Delta to station Beaulieu (all physical and geometrical characteristics can be found in appendix).

In this paper, three wheel profiles are considered: a new one, an intermediate one, and a worn one (Fig. 2).

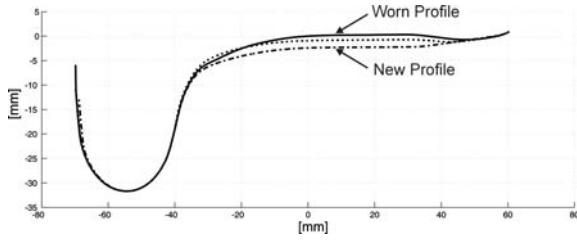


Fig. 2. Contact points between a new rail profile and (a) new wheel profile; (b) a worn wheel profile.

Table II gives the main characteristics of these profiles.

TABLE II
EVOLUTION OF WHEEL PARAMETERS.

Profile	QR [mm]	Sh [mm]	Sd [mm]
New	8.97	31.564	27.104
Intermediate	8.452	31.282	27.103
Worn	8.417	31.012	27.104

Similar tolerances are also given for the wheel radius; its effect on the development of rail corrugation is also discussed in section IV.

III. Steering Capabilities

In curve, the outer rail l_2 is longer than the inner rail l_1 (Fig. 3). As a consequence, outer wheels run a longer path than inner wheels. On the other hand, centrifugal lateral forces impose a lateral displacement of the contact point. Wheel profiles are designed in such a way that this variation of the lateral coordinate is associated with a variation of the vertical coordinate.

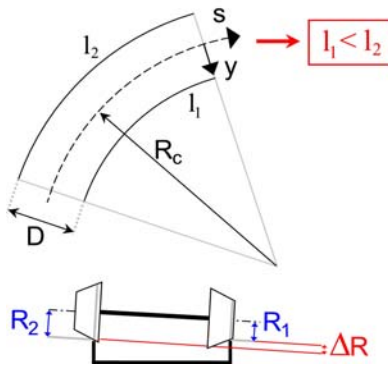


Fig. 3. Simplified drawing of a curved track; Lateral position of the wheel set on the track.

The rolling radius of the outer wheel R_2 (resp. inner wheel R_1) is increased (resp. decreased), tending to compensate the difference of rail length, i.e.

$$\begin{aligned} R_1 &= R_w - \Delta R / 2 \\ R_2 &= R_w + \Delta R / 2 \end{aligned} \quad (1)$$

where $\Delta R = R_1 - R_2$ and R_w is the nominal radius of the wheel. The motion of the wheel set is adapted to the track if

$$\Delta R = DR_w / R_c \quad (2)$$

where R_c is the radius of the curve and D is the distance between contact points. In practice however, it is never the case.

The impact of wheel profile ageing on the steering capability of the vehicle in curve is studied on the test case described in appendix. Three simulations are performed for which the vehicle is successively mounted with wheels having new, intermediate and worn profiles. In straight and curved track (stage 1 and 3 in Fig. 4), all three profiles show the same yaw angles and derailment coefficients (ratio between the lateral and vertical force exerted by the wheel on the track). However, when the vehicle enters and leaves the curve (stage 2 and 4 in Fig. 4), peaks of lateral forces arise when the wheel profile is worn. These come from sudden switches of the contact point from the tread to the flange or the flange to the tread (also shown in [3]).

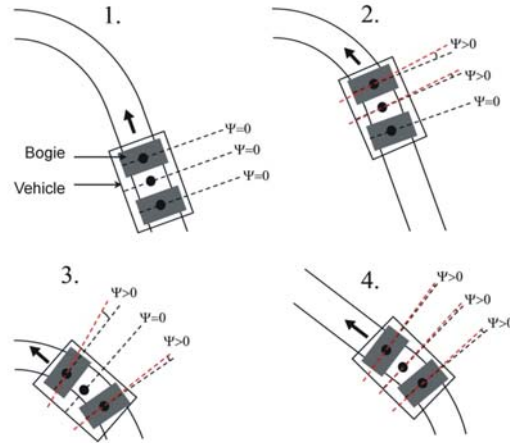


Fig. 4. Four stages of a bogie passing a curve.

IV. Corrugation

IV.1. Wear calculation

In this study, the material loss per unit area Δm is assumed to be proportional to the frictional work density $w_f(x, y)$

$$\Delta m(x, y) = C_w(x, y)w_f(x, y) = C_w \int_0^\tau p_f(x, y)dt \quad (3)$$

with C_w the wear coefficient (usually tuned to $2.5 \cdot 10^{-9}$ Kg/Nm [4]) and τ the time interval a point of the railhead stays in the contact patch. The coordinate axes x and y describe respectively the longitudinal and lateral directions of the contact patch. The frictional power density is defined by the product of the creep force per

unit area and the relative velocity between two bodies in contact. Expressed in terms of the longitudinal (v_x), lateral (v_y) and spin (ϕ) creepages [5], the frictional power is

$$p_f(x, y, t) = \frac{v_m}{\pi a(t)b(t)} (T_x v_x + T_y v_y + M \phi) \quad (4)$$

with v_m the mean velocity of the vehicle; T_x , T_y and M are respectively the longitudinal creep force, lateral creep force and creep torque between the wheel and the rail [4]. Using (4) into (3), the material loss takes the final form

$$\Delta m(x, y) = C_w(x, y) \frac{v_m \tau}{\pi ab} (T_x v_x + T_y v_y + M \phi) \quad (5)$$

The test case considered is a curved track section from the Brussel's subway network, described in appendix. Fig. 5 shows the Short Time Fourier Transform (STFT) of the frictional power density dissipated in the wheel-rail contact of the back wheel set of the front bogie.

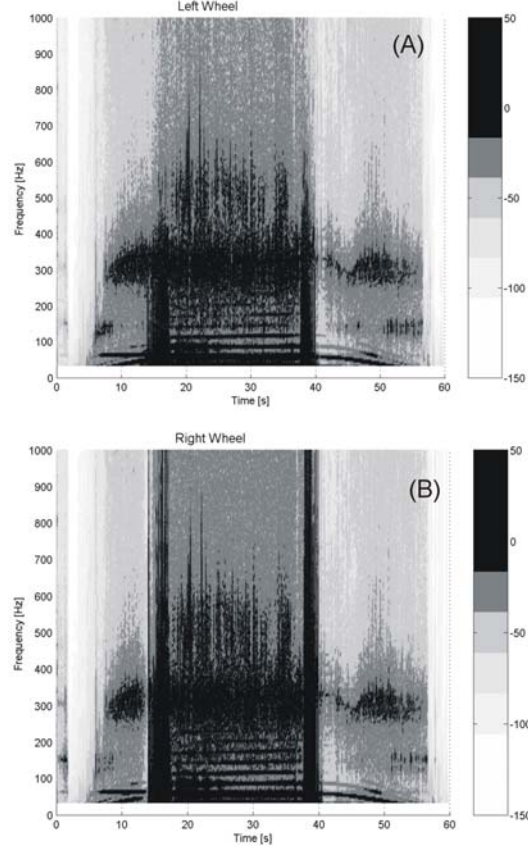


Fig. 5. STFT of the frictional power dissipated in the (a) left and (b) right wheel-rail contact of the back wheel set of the front bogie.

This diagram shows how the Fourier spectrum of the frictional power is changing during the motion of the vehicle. It enters the curve after 15s and leaves the curve after 40s. Dark regions represent peaks of the

spectrum. Two types of excited modes can be distinguished: (i) Thin low frequency peaks, related to track modes and (ii) higher frequency peaks, corresponding to resonance modes of the wheel set [6].

In the following sections, the effect of the wheel shape on these spectral densities is evaluated using the same test case.

IV.2. Effect of wheel profile shape

In this section, three simulations are performed. The test case is the same, and all vehicle wheels successively new, intermediate and old profiles. For each case, the time histories of the frictional power dissipated in the four wheel-rail contacts of the front bogie are calculated. The RMS values of the signals are compared in Fig. 6.

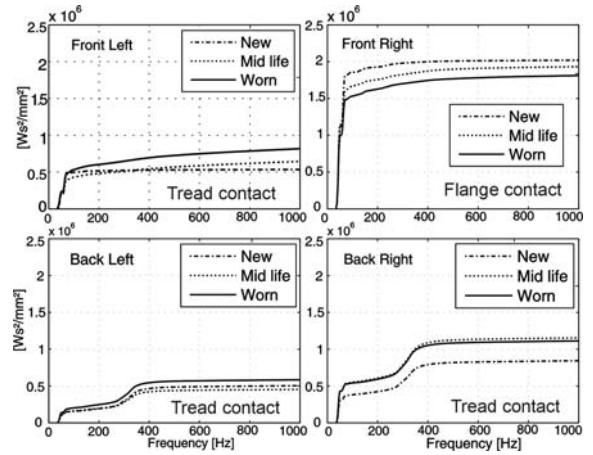


Fig. 6. RMS values of the frictional power dissipated in wheel-rail contacts of the front bogie for new, intermediate and worn profiles.

Fig. 6. shows that: (i) There is a strong (resp. weak) influence of the profile age on the excitation of low (resp. high) frequency modes; (ii) Worn wheel profiles lead to a high conformity between wheel and outer rail, leading to high dissipation and instabilities.

IV.3. Effect of wheel set's wheels diameter difference

The diameter difference allowed between wheels of the same wheel set is $\Delta D_{WS} = D_R - D_L = 2.5 \text{ mm}$. First are studied the variations of ΔD_{WS} of the front wheel set on corrugation. Table III gives the values wheel diameters considered for each simulation of the vehicle passing on the track. All wheels are supposed to have new profiles.

Fig. 7(a) shows, for each contact point, the total amount of energy dissipated in the contact patch at the end of the simulation for an increasing diameter difference. In order to quantify the contribution of the dissipation related to the first torsional and bending mode of the wheel set, Fig. 7(b) shows the same

quantities in the frequency range between 53 Hz and 67 Hz. Fig. 8 shows the same results as Fig. 7 for an decreasing difference of rolling radius.

TABLE III
EVOLUTION OF WHEEL PARAMETERS.

D_R [mm]	D_L [mm]	ΔD_{ws} [mm]	Tread Contact [%]	Flange Conta ct [%]
830	830	0	25	75
830	828.5	+1.5	17.66	82.34
830	828	+2	22.1	77.8
830	826.5	+3.5	36.8	63.2
828.5	830	-1.5	24	76
828	830	-2	24.1	75.9
826.5	830	-3.5	24.66	75.33

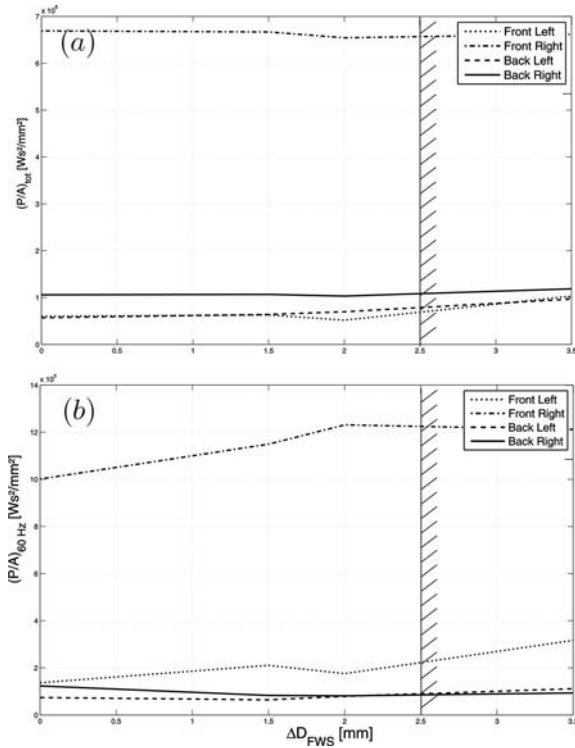


Fig. 7. Energy dissipated in contacts of the front bogie as a function of an increasing diameter difference of the front wheel set (a) in the whole frequency range; (b) between 53 Hz and 67 Hz .

For the test case considered, the diameter difference of has no significant influence on the global energy dissipated for the front wheel set. However, when the diameter difference leaves the zero reference value (in the negative or positive direction), it leads to an increase of 10 to 20 % of total energy dissipated.

The same set of diameter differences (Table III) is applied to the back wheel set. Fig. 9(a) shows, for each contact point, the total amount of energy dissipated in the contact patch at the end of the simulation for an increasing diameter difference and Fig. 9(b) shows the same quantities in the frequency range between 53 Hz and 67 Hz. Fig. 10 shows the same results as Fig. 9 for an decreasing difference of rolling radius.

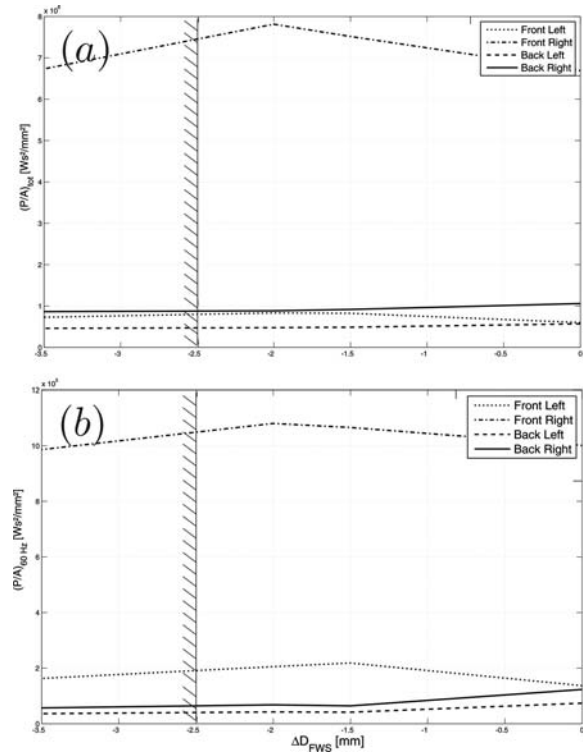


Fig. 8. Energy dissipated in contacts of the front bogie as a function of an decreasing diameter difference of the front wheel set (a) in the whole frequency range; (b) between 53 Hz and 67 Hz .

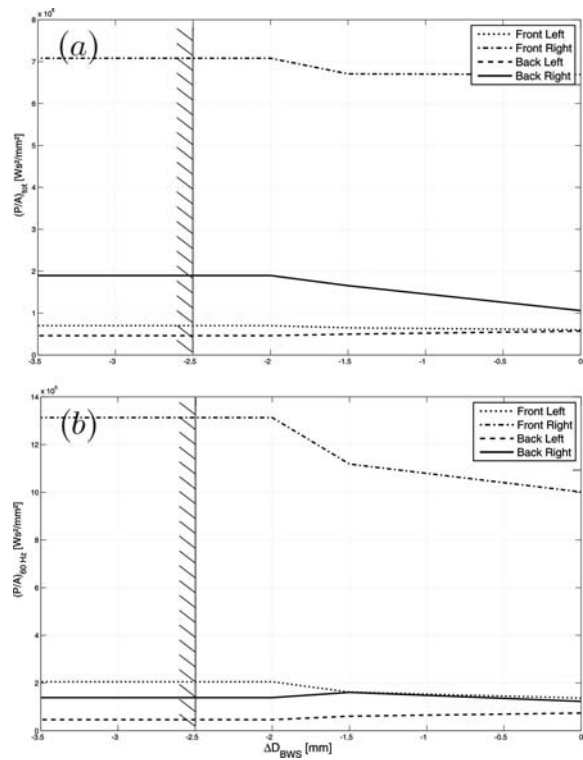


Fig. 9. Energy dissipated in contacts of the front bogie as a function of an decreasing diameter difference of the back wheel set (a) in the whole frequency range; (b) between 53 Hz and 67 Hz .

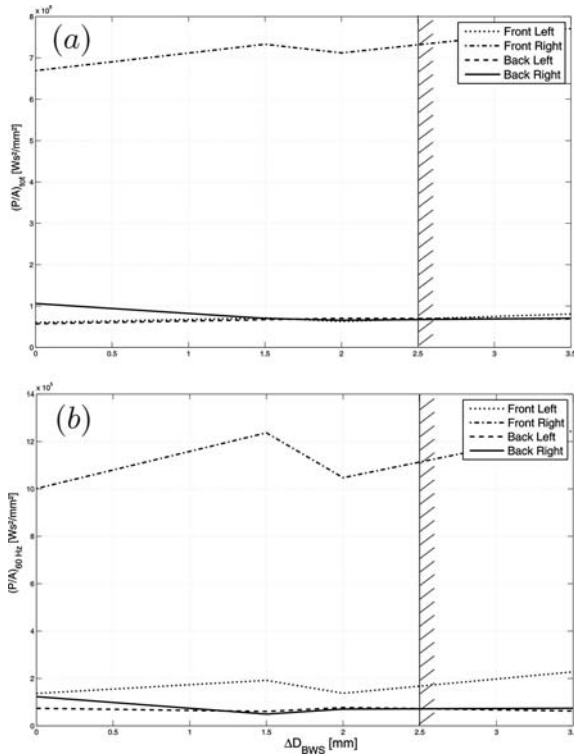


Fig. 10. Energy dissipated in contacts of the front bogie as a function of an increasing diameter difference of the back wheel set (a) in the whole frequency range; (b) between 53 Hz and 67 Hz .

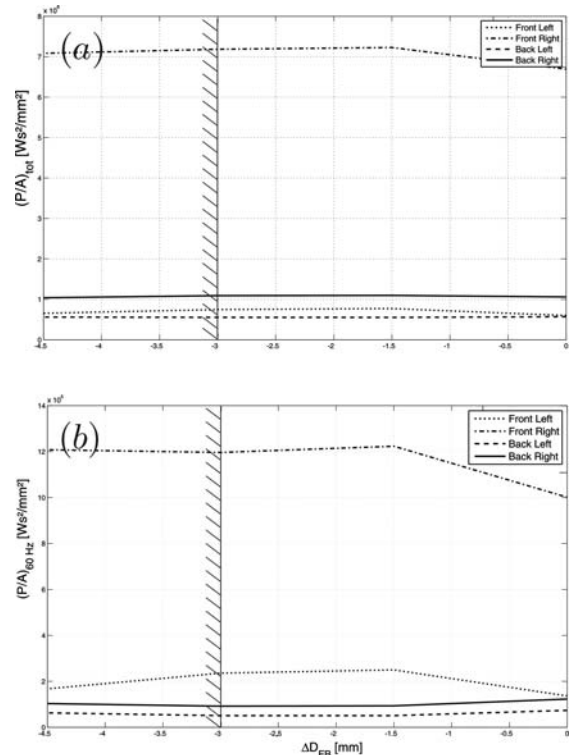


Fig. 11. Energy dissipated in contacts of the front bogie as a function of a decreasing bogie wheels diameter difference (a) in the whole frequency range; (b) between 53 Hz and 67 Hz .

IV.4. Effect of bogie's wheels diameter difference

The allowed diameter difference for wheels from the same bogie is 3 mm. In this study, wheels from the same wheel set have the same radius. Wheel diameter differences $\Delta D_B = D_{FWS} - D_{BWS}$ imposed between front and back wheel set are listed in Table IV.

TABLE IV
EVOLUTION OF WHEEL PARAMETERS.

D_{FWS} [mm]	D_{BWS} [mm]	ΔD_B [mm]	Tread Contact [%]	Flange Conta ct [%]
830	830	0	25	75
830	828.5	+1.5	23.3	76.7
830	827	+3	23.42	76.58
830	825.5	+4.5	23.2	76.8
828.5	830	-1.5	23.4	76.6
827	830	-3	23.5	76.5
825.5	830	-4.5	23.6	76.4

Fig. 11(a) shows, for each contact point, the total amount of energy dissipated in the contact patch at the end of the simulation for an increasing diameter difference and Fig. 11(b) shows the same quantities in the frequency range between 53 Hz and 67 Hz. Fig. 12 shows the same results as Fig. 11 for an decreasing difference of rolling radius.

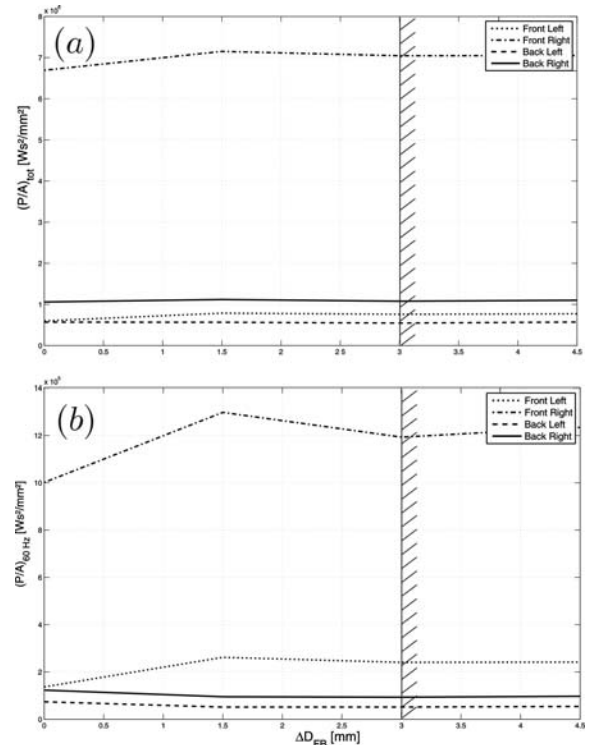


Fig. 12. Energy dissipated in contacts of the front bogie as a function of an increasing bogie wheels diameter difference (a) in the whole frequency range; (b) between 53 Hz and 67 Hz .

A positive or negative diameter difference has an effect of increasing the total amount of energy loss in contact patch of the front wheel set, and the opposite effect for the back wheel set. This conclusion is valid for the total energy loss as well as for a frequency range restricted between 53 Hz and 67 Hz. However, these variations are quite small and related to very small changes in the diameter differences. For differences above 1.5 mm, no influence of the wheel diameter difference is visible anymore.

IV.5. Effect of vehicle's wheels diameter difference

The tolerance for wheels from the same bogie is 14 mm. In this study, wheels from the same bogie have the same radius. Diameter differences $\Delta D_V = D_{FB} - D_{BB}$ listed in table V are successively imposed between front and back bogie.

TABLE V
EVOLUTION OF WHEEL PARAMETERS.

D_{FB} [mm]	D_{BB} [mm]	ΔD_V [mm]	Tread Contact [%]	Flange Conta ct [%]
830	830	0	25	75
830	823	+7	23.2	76.8
830	816	+14	23.3	76.7
830	809	+21	23.2	76.8
823	830	-7	23.2	76.8
816	830	-14	22.7	77.3
809	830	-21	22.6	77.4

Fig. 14(b) shows, for each contact point, the total amount of energy dissipated in the contact patch at the end of the simulation for a decreasing diameter difference and Fig. 14(b) shows the same quantities in the frequency range between 53 Hz and 67 Hz. Fig. 15 shows the same results as Fig. 14 for an increasing difference of rolling radius.

The influence of the wheel radius difference between bogies on rail corrugation is rather small. Actually, due to the isolation of the un-sprung mass through the primary and secondary suspension, differences in geometrical properties between bogies do influence the global dynamics of the vehicle in the low frequency range rather than in the frequency range in concern for the study of rail corrugation.

V. Conclusion

In this paper, a parameter study has been performed in order to evaluate the impact of wheel profile ageing on the development of rail corrugation in curve. This study has been performed using a multi-body model of the vehicle track system with data set from the Brussels subway network. In the first part of the paper, it has been shown that worn profiles lead to a higher

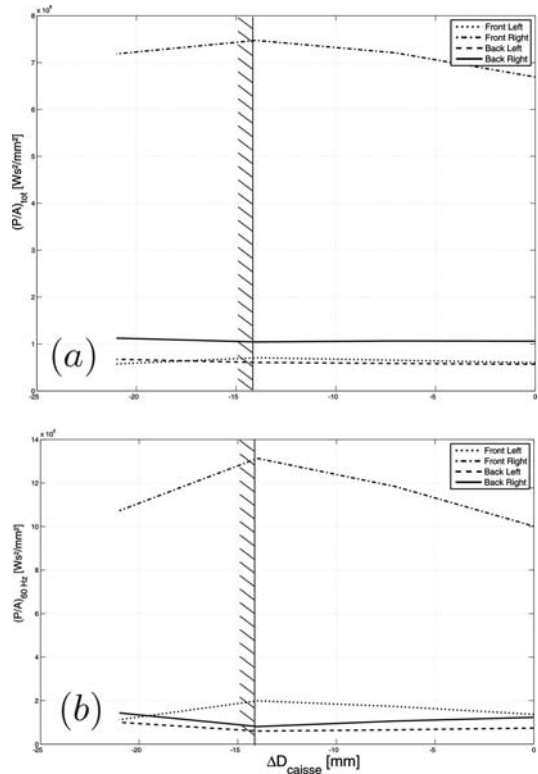


Fig. 14. Energy dissipated in contacts of the front bogie as a function of an increasing diameter difference of the back wheel set (a) in the whole frequency range; (b) between 53 Hz and 67 Hz

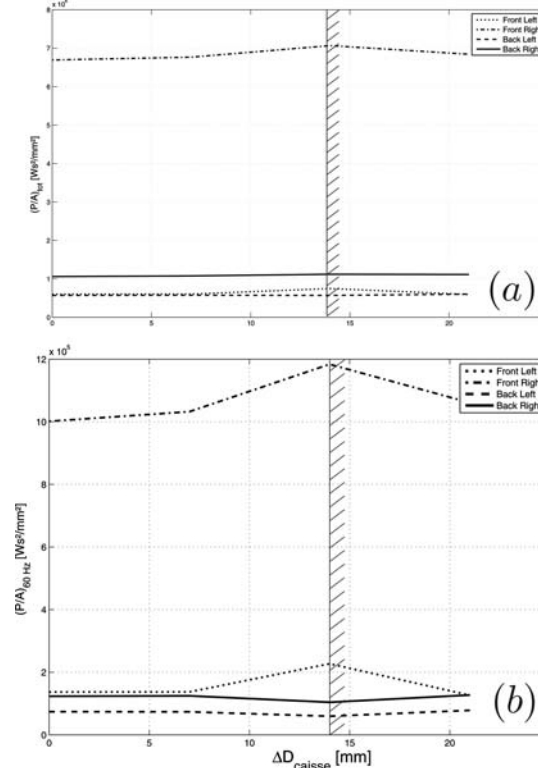


Fig. 15. Energy dissipated in contacts of the front bogie as a function of an increasing diameter difference of the back wheel set (a) in the whole frequency range; (b) between 53 Hz and 67 Hz .

conformity between the wheel and the rail, leading to switches of the contact patch and instabilities. It results in a strong (resp. weak) influence of the profile age on the excitation of low (resp. high) frequency modes.

In the second part of the paper, the impact of the wheel radius has been investigated. It has been shown that the wheel radius has a great influence on the total amount of frictional power dissipated in the contact patch. A decrease of 3 cm of the wheel diameters of the vehicle engenders an increase of 10 to 20 % of the total amount of energy loss in the contact patches. As a consequence of these better predictions, mainly two recommendations are given to decrease the contribution of the railway wheel profile in the development of rail corrugation. Recommendation 1: more strict tolerance for the wheel radius could able to save energy and decrease the global dissipation of energy in the contact patch.

Regarding all the other criteria related to the wheel diameter, it appears that the influence of wheel radius changes on energy dissipation in contact points of the back wheel set is quite weak. Consequently, tolerances for these wheels are strict enough against rail corrugation. However, any change in diameter of wheels of the front wheel set increases the frictional power dissipated.

Recommendation 2: apply stricter tolerances for wheels of the first wheel set (front wheel set of the front bogie and back wheel set of the back bogie).

Appendix

Fig. 16 depicts the track section chosen from the Brussel's subway network. It consists of a sharp curve of 175 m radius, starting from station Detla to station Beaulieu. Some corrugated wavelengths are also specified, associated with the date they were measured. As an example, Fig. 17 shows a picture of a corrugated rail with a wavelength of 6 cm.

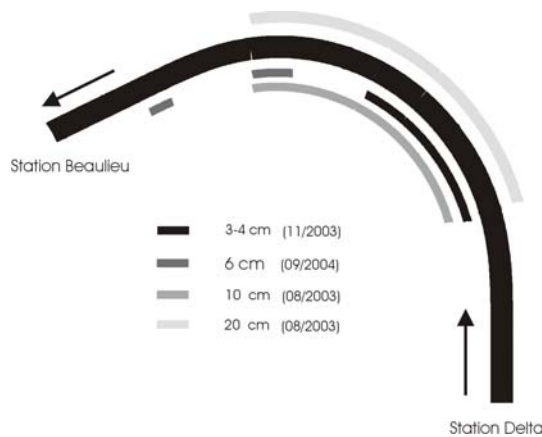


Fig. 16. Simplified drawing of Brussel's subway track section considered for the study; Wavelengths of observed corrugation and place where it appears on the inner and outer rail are also mentioned.

The track is modelled with two layers of spring-mass-damper elements, following the wheel set above them [6].

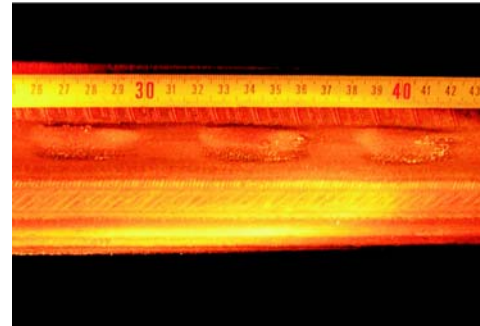


Fig. 17. Picture of a corrugated rail.

The vehicle is constituted of two bogies, fixed on a carbody through the secondary suspensions. On each bogie, two wheel sets are fixed through the primary suspensions. Fig. 18 shows a picture of the model. A finite element model of the axle represents wheel set flexibility. Resonance frequencies and mode shapes of the wheel set are calculated using the finite element module FEMBS during a pre-processing stage [7], and are compared with measured frequencies in Table VII.

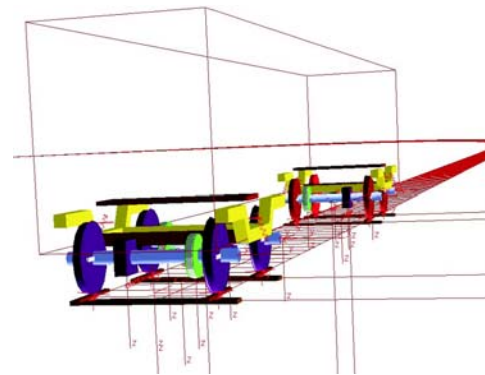


Fig. 18. Multi-body model of the vehicle-track system.

TABLE VII
CALCULATED AND MEASURED RESONANCES OF THE WHEEL SET.

Mode	Model [Hz]	Measurement [Hz]
1st bending mode	63	67
2 nd bending mode	156	178
1st torsional mode	70	73
2 nd torsional mode	310	318

Creep forces between rail and wheel are calculated with the simplified theory of Kalker [8], implemented using

the FASTSIM algorithm [9]. Calculation is achieved using only one contact point per wheel. Rail irregularities (vertical, lateral and spin) are introduced via their power spectral density [6]. Vehicle and track parameters of the multi-body model of the vehicle track system are given in Table VII.

TABLE VIII
VEHICLE-TRACK PARAMETERS FOR THE MULTI-BODY MODEL

Parameter	Value
Wheel profile	U 69
Rail Profile	EB 50 T
Train speed	60km/h
Curve radius	175m
Superelevation	150mm
Track gauge	1500mm
Sleeper spacing	600mm
Car body mass (with passengers)	29740kg
Car body moment of inertia in roll	71000kgm ²
Car body moment of inertia in pitch	821000kgm ²
Car body s moment of inertia in yaw	821000kgm ²
Bogie mass	4560kg
Bogie moment of inertia in roll	1863kgm ²
Bogie moment of inertia in pitch	2537kgm ²
Bogie moment of inertia in yaw	4400kgm ²
Mounted Wheelset Mass	1592kg
Secondary Suspension Lateral stiffness	821000kgm ²
Secondary Suspension Vert. stiffness	838,775kN/m
Secondary Suspension Lat. damping	40kNs/m
Secondary Suspension Vert. damping	14kNs/m
Primary Suspension Long. stiffness	5,2MN/m
Primary Suspension Lat. stiffness	5,2MN/m
Primary Suspension Vert. stiffness	3,9MN/m
Primary Suspension Long. damping	4kNs/m
Primary Suspension Lat. damping	4kNs/m
Primary Suspension Vertical damping	3kNs/m
Rail pad Vertical stiffness	125MN/m
Rail pad Lateral Stiffness	37,5MN/m
Rail pad Vertical Damping	20kNs/m
Rail pad Lateral Damping	0,4kNs/m
Ballast Vertical stiffness (inner)	52,5MN/m
Ballast Lateral Stiffness (inner)	17,5MN/m
Ballast Vertical Damping (inner)	30kNs/m
Ballast Lateral Damping (inner)	15kNs/m

Acknowledgements

The authors would like to acknowledge the Brussels metro network (STIB) for supplying the sites and the European Community for supporting and funding this work under the fifth framework program (project *Wheel-rail corrugation in urban transport* - GRD2-2001-5006).

References

- [1] I.Y. Shevtsov, V.L. Markine, C. Esveld, Optimal design of wheel profile for railway vehicles, *Wear*, Vol. 258, pp. 1022-1030, 2005.
- [2] E.E. Magel, J. Kalousek, The Application of Contact Mechanics to Rail Profile Design and Rail Grinding. *Wear*, Vol. 253, pp. 308-316, 2002.

- [3] S. Mace, R. Pena, N. Wilson, D. Dibritto, Effects of Wheel-rail contact geometry on wheel set steering forces, *Wear*, Vol. 191, pp. 204-209, 1996.
- [4] J.C.O. Nielsen, Numerical prediction of rail roughness growth on tangent railway tracks. *Journal of Sound and Vibration*, Vol. 267, pp. 537-548, 2003.
- [5] S.L. Grassie, J. Kalousek, Rail Corrugation: Characteristics, Causes and Treatments. *Journal of Rail and Rapid Transit*, Vol. 207, pp. 57-68, 1993.
- [6] SIMPACK Manual, Realise 8.6
- [7] K. Popp, H. Kruse, I. Kaiser, Vehicle-Track Dynamics in the Mid-Frequency Range. *Vehicle System Dynamics*, Vol. 31, pp. 423-464, 1999.
- [8] J. Kalker, Survey of Wheel-Rail Contact Theory. *Vehicle System Dynamics*, Vol. 5, pp. 317-358, 1979.
- [9] J. Kalker, A Fast Algorithm for Simplified Theory of Rolling Contact. *Vehicle System Dynamics*, Vol. 11, pp. 1-13, 1982.

Authors' information

¹University of Brussels, Department of Mechanical Engineering and Robotics. 50 av. F.D. Roosevelt, 1050 Brussels, Belgium.

² University of Brussels, Department of Mechanical Engineering and Robotics. 50 av. F.D. Roosevelt, 1050 Brussels, Belgium.